

Asphalt from co-hydrogenation of coal and catalytic cracking residue

Yongbing Xue, Jianli Yang, Zhenyu Liu, Zhiyu Wang

State Key Laboratory of Coal Conversion, Institute of Coal Chemistry, Chinese Academy of Sciences, P.O. Box 165, Taiyuan, Shanxi 030001, P.R. China

Introduction

Coal, as a primary energy resource and air pollution source in China, is demanded to be used as efficient and clean as possible. Catalytic cracking residues (CCR) from petroleum refineries, with an annual production of more than 2 million tones in China, is difficult to be further processed because it contains large amounts of aromatics and heavy metals. Recently, it has been demonstrated that asphalt produced by hydrogenation of coal with CCR may be used as high grade paving asphalt¹⁻⁴. This is important since the need of high grade paving asphalt is increasing with the fast growing of the highway construction in China. In addition, oil can also be produced to make the co-hydrogenation process economical. In this paper, asphalt produced from hydrogenation of Yanzhou coal with three CCRs was studied. The yield, and the chemical and rheology properties of the asphalt were included.

Experimental

Yanzhou coal from Shandong China was used, its properties are listed in Table 1. Three catalytic cracking residues named as CCR1, CCR2 and CCR3 were used. CCR1 and CCR2 were from Shijiazhuang petroleum refinery and CCR3 was from Shenghua petroleum refinery. The properties of the CCRs are given in Table 2. An iron catalyst was impregnated on the coal. The hydrogenation was carried out at 400 °C for 1 hour under a hydrogen pressure of 7 MPa (cold) in an 1-liter autoclave.

Table 1. The proximate and ultimate analyses of Yanzhou coal

Proximate anal. wt%			Ultimate anal. wt%				
Mad	A _{ad}	V _{daf}	C _{daf}	H _{daf}	O* _{daf}	N _{daf}	S _{daf}
2.5	6.7	43.9	80.8	5.1	1.2	3.7	9.2

*: by difference; ad: air dry; daf: dry ash free.

Table 2. The properties of the catalytic crack residue(CCR)

	Ultimate analysis wt%				
	C	H	O	N	S
CCR1	88.92	8.12	0.37	0.32	1.14
CCR2	87.81	9.34	0.36	0.41	0.96
CCR3	85.33	10.88	0.48	0.25	0.96

	Group compositions wt%			
	Saturates	aromatic	resin	asphalte
CCR1	8.1	60.4	27.3	4.2
CCR2	39.36	36.82	18.24	5.58
CCR3	10.07	35.00	33.38	21.55

The hydrogenation products were separated into residues, preasphaltene and toluene solubles by using tetrahydrofuran (THF) and toluene as extraction solvent¹. Asphalt was obtained by distilling out the light products from the toluene solubles.

Thin layer chromatograph coupled with a flame ionized detector (TLC-FID) was used for group composition analysis. Hexane,

toluene, and trichloromethane(95%) + methanol (5%) were used to separate the asphalt into four compositions: saturates, aromatics, resin and asphaltenes. The rheology properties were measured by Cannon Rotary Viscometers.

Results and Discussion

Effects on conversions and yields: The coal and the CCRs were hydrogenated at the reaction conditions separately. Results are shown in Figure 1. It can be seen that both the THF conversion and the asphalt yield of the coal and the CCRs are significantly different. All the CCRs show high THF conversions (>95%) and high asphalt yields.

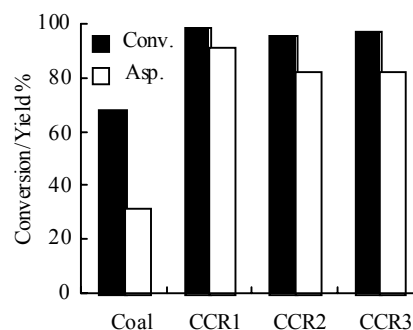


Fig. 1 Conversion/Yield of coal and CCRs

Co-Hydrogenation of the coal and a CCR was carried out at different coal-to-CCR ratios. Synergic effect on the asphalt yield is defined as the difference in asphalt yield between experimental data and the theoretical calculation. The theoretical calculation was made through mathematical addition of the results from individual hydrogenation runs weighted by the coal-to-CCR ratio. Figure 2 gives the experimental and calculated asphalt yields along with the synergic effects for the co-hydrogenation of Yanzhou coal with CCR1. The co-hydrogenation results of the coal and the other two CCRs are similar.

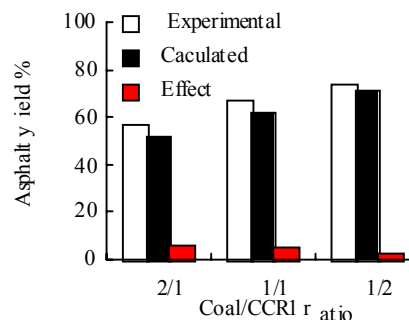


Fig. 2 Asphalt yields and synergic effects

Compared to the hydrogenation of the coal and the CCR alone, the synergic effect is obvious although the effect level is different for different CCRs. The main reason may be that the CCR is not only functioning as a reactant but also a reaction solvent during the co-hydrogenation. Coal particles can be solved, swollen and dispersed by the reaction solvent. Hydrogen can be supplied and transferred by a hydrogen donor solvent⁵. All the three CCRs contain over 30% aromatic compounds. The group compositions (see Table 2) are closed to that of the coal liquids. From chemistry point of view, these CCRs are good hydrogen transfer and coal dissolution solvents.

Effects on group compositions of the asphalt: Results of group composition analysis for the asphalt produced are given in Table 3. Generally, saturates and aromatics increase with the increase of the CCR concentration in the feed stock. Resin and asphaltenes decrease with the increase of the CCR concentration. These results suggest that the saturates and aromatics are mainly from CCRs and resins asphaltenes are mainly from the coal.

Table 3. The group compositions of the asphalt produced

	Coal:CCR	Saturates	Aromatics	Resin	Asphaltene
CCR1	2:1	4.90	12.80	57.20	25.70
	1:1	5.13	24.51	59.05	11.31
	1:2	25.07	29.92	29.83	15.18
CCR2	2:1	16.73	13.39	44.57	25.31
	1:1	26.63	14.82	34.28	21.77
	1:2	10.92	18.10	52.78	18.20
CCR3	2:1	3.04	6.21	60.88	29.87
	1:1	35.94	17.33	33.12	13.61
	1:2	45.53	27.15	23.27	4.05

In the view of paving asphalt⁶, saturates components worsen asphalt property. The less the saturate content is, the better the asphalt quality is. The saturate concentration must be controlled to a limited amount in high grade paving asphalts. Aromatic component can dissolve micelles formed by resins and asphaltenes and is a necessary component to make asphalt in the sol-gel state that has high viscous-elastic effects. Resin is the key component for the good viscous-elastic property. Asphaltenes act as enters for promoting the formation of the micelles. It also adsorbs resin. So a certain amount of asphaltenes is also necessary to form micelles. But excessive amount of asphaltenes will result to low penetration, high softening point and low ductility. In fact, the first two products listed in Table 3 (rows 2 and 3) have demonstrated their satisfaction in meeting the Chinese National Standard (GB/T 15180-94) for high grade paving asphalt in terms of penetration, softening point and ductility.

Rheological properties of the asphalts: Rheology properties are important in determination of asphalt application, especially in road paving⁷. The changes in viscosity of a number of asphalts with temperature at a number of spin rates were measured. Figure 3 shows viscosities of three asphalts, a commercial product and two co-hydrogenation products, at various temperatures and a spin rate of 1 rpm. The latter two were obtained from co-hydrogenation of Yanzhou coal with CCR1 and CCR2 at a coal-to-CCR ratio of 1/1.

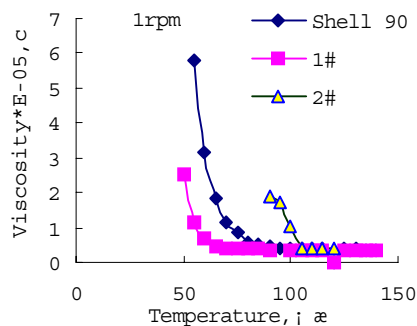


Fig. 3 Viscosity of asphalts

Generally, viscosities of the asphalts decrease with increases in temperature and in spin rate, but the temperature ranges where the viscosity changes the most are different. The curve in Fig. 3 for asphalt #1, which meets the Chinese national standard for high way asphalt, falls in the left side of Shell 90; while the curve for asphalt #2, which does not meet the Chinese national standard for high way

asphalt, falls in the right side of Shell 90. Clearly, The rheological properties of the co-hydrogenation asphalts can be controlled by varying CCRs and the hydrogenation conditions. It is important to point out that, compared to Shell 90, no additives were added in the co-hydrogenation asphalts.

4. Conclusions

Co-hydrogenation of Yanzhou coal and CCR at mild conditions may produce asphalt with properties similar to that of petroleum derived high quality paving asphalt. Synergetic effects in asphalt yield hydrogenation of the coal and the CCR, the asphalt yield was enhanced greatly. The properties of the asphalt produced can be controlled by adjusting the CCR and the co-hydrogenation conditions. High aromatic CCR can produce asphalt of good rheology properties to meet the highway requirements.

Acknowledgement: The authors gratefully acknowledge the financial support from the National Natural Science Foundation of China, the Chinese Academy of Sciences, and the Special Funds for Major State Basic Research Project. Mr. Yanti Wang of Shijiazhuang petroleum refinery is also acknowledged.

References

1. Yunmei Li, Ruiping Yan, Jianli Yang, Zhenyu Liu, Zhe Wang, Proceedings of The 14th Annual International Pittsburgh Coal Conference & Workshop, 1997, CD-ROM
2. Hong Cui, Jianli Yang, Yunmei Li, Yongda Gu, Zhenyu Liu, Proceedings of The 14th Annual International Pittsburgh Coal Conference & Workshop, 1997, CD-ROM
3. Zhenyu Liu, Jianli Yang, Proceedings of The 15th Annual International Pittsburgh Coal Conference & Workshop, 1998, CD-ROM
4. Zhijie Wang, Ruiping Yan, Yunmei Li, H. Zhang, J. Yang, Z. Liu, 3rd China-Korea Joint Workshop on Coal & Clean Energy Utilization Technology, taiyuan, Shanxi, P.R.China, 2000
5. Yongbing Xue, Kaicheng Lin, Gangming Zou, Coal Conversion 22(3): 1-4, 1999
6. Edwin J. Barth, Asphalt science and technology, Gordon and Breach Science Publishers, New York 1962
7. D. Mastrofini, M. Scarsella, Fuel 79(2000),1005-1015

EFFECT OF PRE-REDUCTION ON CARBON FORMATION DURING STEAM REFORMING OF METHANE OVER PROMOTED AND UNPROMOTED Ni/Al₂O₃ CATALYSTS

Jian Zheng, Wei Pan, Chunshan Song*

Clean Fuels and Catalysis Program, Energy Institute and Department of Energy & Geo-Environmental Engineering, Pennsylvania State University, University Park, PA 16802
Email: csong@psu.edu; Tel: 814-863-4466; Fax: 814-865-3248

Introduction

The steam reforming of methane is a well established industrial process for the production of synthesis gas (CO + H₂)¹. The reaction is favored at high temperature, where coke formation is also a problem². As a result, nickel – the most cost-effective catalyst – is loaded on support material with additional promoters that catalyze gasification of carbon (coke or of intermediates leading to coke). Potassia³ and magnesia¹ etc are known to promote gasification by steam. However, catalyst deactivation due to carbon deposition still exists in industrial production after several months or years reforming reactions even with high steam/carbon ratio⁴.

Many studies have been done on the mechanism of carbon formation and the promoting effect of basic alkali, alkaline earth metal oxides for decreasing of coke formation³. However, most of the studies concentrated on what happened on the surface of Ni metals, since most of the catalysts had been reduced at high temperature to achieve fully reduction. Little is known therefore about the effect of un-reduced Ni on the catalytic properties and carbon formation.

Based on a previous research, a pretreatment procedure, where the Ni supported catalysts were pre-reduced at 450°C, was found to give good catalyst performance⁵. However, the reduction of NiO may become more difficult in the presence of Ca or K, etc. Therefore, this work aims at studying the effects of pre-reduction of K₂O and CaO promoted Ni/Al₂O₃ catalyst on the reforming catalysts and carbon formation. This kind of study may shed some light on the causes of and ways to eliminate carbon formation.

A commercial reforming catalyst promoted with K₂O and CaO was chosen in this study for the steam reforming of methane at different temperatures with different pre-reduction treatments. Interesting results have been found that carbon formation is more severe in the case of partially reduced Ni catalysts.

Experimental

Sample. Two commercial catalysts were obtained from Süd Chemie, one is the un-promoted (C11-9-09) with 1-15% NiO, 85-99% Al₂O₃ (as per the data provided by vendor) and the other is the promoted (G-91) with 15-25% NiO, 45-60% Al₂O₃, 5-15% CaAlO₂, 5-15% CaO and 1-10% K₂O.

Characterization. XRD patterns of the catalysts were obtained using a Scintag powder Diffractometer with Cu K α as the radiation source. The reduction of the fresh catalysts were characterized by conventional TPR with a heating rate of 10°C/min in argon (Ar, 30 ml/min). H₂-TPD was carried out on the catalysts reduced in situ at different temperature followed by purging with Ar. TPD profiles were then recorded by TCD detector at 10°C/min in Ar. Carbon formation on the used catalysts was characterized by using a highly sensitive LECO RC-412 Multiphase Carbon Determinator, where the CO₂ produced during TPO was monitored by means of IR. SEM/EDX was also done for the information of surface images and compositions of used catalysts using HITACHI S-3500N Scanning Electron Microscope.

Reforming. The reaction of steam reforming of CH₄ was studied at three different temperatures, 450°C (842°F), 538°C (1000°F) and 649°C (1200°F), under pressure of 200 psi (13.6 atm) with the feed H₂O/CH₄ molar ratio of 0.5. Space velocity (WHSV) was kept at 30,000 cm³.g⁻¹.h⁻¹. About 0.1g catalyst sample was placed in the middle of an Inconel 800 H alloy tubular reactor (0.54" O.D. x 0.375" I.D. and about 16" in length). α -Al₂O₃ spheres (2 mm I.D.) were filled up to the rest of the reactor.

Before admitting the reactants the catalysts were pre-reduced in H₂ (10 ml/min)-Ar gas flow (30 ml/min) at different temperature for 75 min. Then the reaction run was started by introducing H₂O followed by CH₄ feed (10 ml/min). A condenser was used to remove un-reacted H₂O after the reaction. Reaction products were analyzed by on-line GC (SRI GC 8610C) using a packed silica gel column and TCD detector. GC data were recorded every 30 min during a time-on-stream (TOS) period of 300 min after the steady state conditions were reached (15-30 min).

Results and Discussion

An intense XRD peak attributing to the diffraction of NiO (012) still exists on the promoted G-91 catalyst after reduction at 450°C, which disappears at higher reduction temperature.

TPR profiles as shown in **Figure 1** confirm that the promoters (K₂O and CaO) make the reduction of NiO harder. In the absence of promoter (curve **a**), the reduction of NiO starts at 300°C and peaks at 460°C, so the pretreatment procedure that we developed previously⁵ is suitable to achieve full reduction of NiO. On the contrary, the reduction of same metal oxide over G-91 catalyst could not occur until temperatures higher than 400°C, and the T_{max} of the first TPR peak (curve **b**) is around 500°C. A second TPR peak appears and is probably due to the reduction of less reducible NiO-CaO-K₂O solid solution. Therefore, partly reduced NiOx (x \leq 1) remains after pre-reduction at 450°C.

H₂-TPD of G-91 catalyst after 450°C reduction shows relatively smaller peak at around 120°C than those reduced at higher temperature (figures not shown). However, two additional H₂-TPD peaks at higher temperature (350°C and 600°C) can be found in the case of 450°C reduction, which might be due to the desorption of H₂ bounded to NiOx during the purging process in Ar.

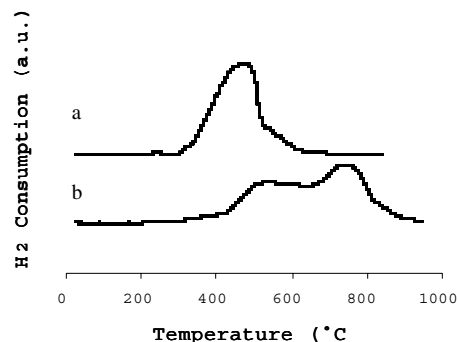


Figure 1. TPR profiles of un-promoted C11-9-09 (a) and promoted G-91 (b) catalysts.

Table 1. Results of Methane Steam Reforming on G-91 Catalysts (H₂O/CH₄: 0.5, 200 psi, TOS: 5 h)

T _{rex} (°C)	450		538			649		
	T _{red} (°C)		T _{red} (°C)			T _{red} (°C)		
	450	850	538	649	850	450	649	850
Conv (%)	25.1	17.3	14.6	7.1	28.7	22.9	24.0	23.4
Yield								
H ₂	6.5	6.6	15.0	12.0	13.0	27.5	27.2	28.3
CO	0	0	0	0	0	4.2	3.8	4.4
CO ₂	3.3	3.5	7.3	2.2	6.2	9.1	9.5	9.7

* T_{rex}: Reaction temperature, T_{red}: Pre-reduction temperature.

Steam reforming catalysis results of G-91 catalyst (TOS = 5 h) are listed in **Table 1**. There are no big differences among the activity and product yields of the same catalyst after different pre-reduction treatments, especially at reaction temperature of 649°C. This is probably because that the H₂ produced during the steam reforming will eventually reduce the NiOx to Ni, which therefore acts as the same active sites for methane steam reforming as the case of pre-reduction at higher temperature.

However, it is worth noting that, there is a trend of the decreasing amount of carbon deposition with the increase of pre-reduction temperature as analyzing the used catalysts by TPO-IR.

Figure 2 shows the TPO-IR patterns of G-91 catalyst pre-reduced at different temperature followed by 5 h reforming reaction of methane at 649°C. Several peaks are presented in all samples, as noticing that the curves in Figure 2 are drawn in different scales. The amount of the peaks at lower temperature (<400°C) almost keep constant in all cases, which are probably due to the desorption of CO₂ chemisorbed on Ni supported catalysts during reforming reaction. Therefore these peaks may not relate directly to the carbon deposited. The peak with T_{max} at 600°C is the oxidation of carbon filament, which is in accordance with literature work⁶.

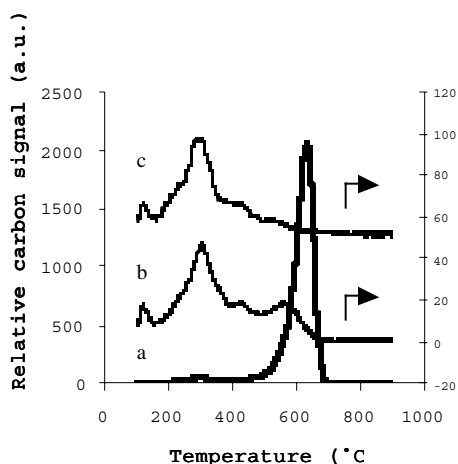


Figure 2. TPO-IR spectra of G-91 catalyst pre-reduced at 450°C (a), 649°C (b), and 850°C (c) followed by steam reforming of methane at 649°C for 5 hours.

It is very interesting to note that the amount of filament carbon significantly increases with decreasing temperature of pre-reduction, especially at reduction temperature of 450°C where NiO has not been fully reduced.

This observation indicates that formation of carbon filament can be enhanced on partially reduced NiOx/Al₂O₃ catalyst when compared to fully reduced Ni/Al₂O₃ catalyst.

Figure 3 shows the SEM pictures of the used G-91 (after 5 h TOS) catalysts that were pre-reduced at 450°C and 649°C, respectively. Significant amount of carbon filament can be easily found in the case of lower-temperature pre-reduction, while it is less obvious in the case of higher reduction temperature.

All these results seem to correlate well with each other. Although the partially reduced NiOx in the promoted reforming catalyst can be eventually fully reduced under high temperature reaction conditions, certain species in partially reduced catalyst may act as an active site for the initial carbon formation, which could be accumulated to become severe. Therefore, care should be taken to achieve full reduction of the promoted Ni catalysts before the reforming reaction, particularly when using lower steam/carbon ratios.

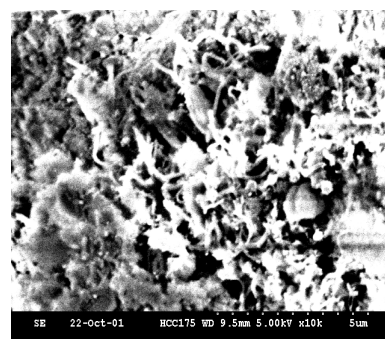
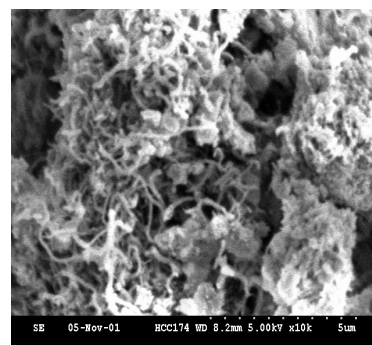


Figure 3. SEM pictures of G-91 catalyst pre-reduced at 450°C (above) and 649°C (below) followed by steam reforming at 649°C for 5 hours.

Conclusions

The present work reveals that there is a significant effect of pre-reduction treatment on the carbon formation during steam reforming of methane over promoted Ni/Al₂O₃ catalyst. The partially reduced catalyst enhances carbon formation when compared to fully reduced catalyst, possibly because some species

in partially reduced catalyst (NiOx?) acts to promote the initial carbon formation.

Acknowledgement. We are grateful to Air Product and Chemicals Inc. and to the Pennsylvania State University for partial financial supports. We also wish to thank United Catalyst Inc./Süd Chemie for providing the catalyst samples. JZ would like to thank Dr. M. Klimkiewicz for help with the use of SEM/EDX, to Ms. N. Wonderling for help in the XRD, and to Dr. A. Orhan for help with the use of TPO-IR instrument.

References

- (1) Rostrup Nielsen, J. *Steam Reforming Catalysts*, **1975**, Danish Technical Press, Copenhagen.
- (2) Bartholomew, C. H. *Catal. Rev. - Sci. Eng.*, **1982**, *24*, 67-112.
- (3) Trim, D. L. *Catal. Rev. - Sci. Eng.*, **1977**, *16*, 155-167.
- (4) Arakawa, H.; et al. *Chem. Rev.*, **2001**, *101*, 953-996.
- (5) Song, C., Murata, S., Srinivas, S.T., Sun, L., Scaroni, A.W. *Am. Chem. Soc. Div. Petrol. Chem. Prepr.*, **1999**, *44*, 160.
- (6) Wang, S.; Lu, G. Q. *J. Chem. Tech. Biotechnol.*, **2000**, *75*, 589-595.

HYDRODEMETALLATION OF NICKEL AND VANADYL OCTAETHYLPORPHYRINS IN THE ABSENCE OF A CATALYST

Hai Xu, Daoyong Yu, Guohe Que, Zongxian Wang

State Key Laboratory of Heavy Oil Processing, Faculty of Chemistry
and Chemical Engineering, University of Petroleum, Dongying
257061, China

Introduction

Metals in petroleum (mainly nickel and vanadium) often cause serious problems in the catalytic cracking and the hydrodesulfurization units, such as blocking the pores, fouling the active sites and changing the selectivity of the catalyst. So it is necessary to remove these metals in advance. And a better understanding of the chemical properties of metal containing compounds in petroleum would lead to develop an effective and economic demetallation process.

At present, as only some nickel and vanadyl porphyrins have been isolated from petroleum and identified, and a little is known about other metal containing compounds, so most of demetallation studies have been devoted to metal porphyrins. Many investigators (1-4) have studied the catalytic hydrodematllation of nickel and vanadyl porphyrins and a sequential HDM mechanism has been proposed, but the demetallation reaction mechanism in the absence of a catalyst seems to be unclear. In the present study, the demetallation reaction mechanism of nickel and vanadyl 2,3,7,8,12,13,17,18-octaethylporphyrins (NiOEP and VOOEP) in the absence of a catalyst at temperature from 613 to 653 K and pressure of 3 and 9 MPa H₂ is described.

Experimental

NiOEP and VOOEP (Aldrich, >97%) were employed as model compounds. A liquid paraffin free of sulfur, nitrogen and metals was used as a solvent and purchased from Beijing Chemicals. The method of dissolving the model compounds in the liquid paraffin was based on the description by Hung and Wei (1).

All experiments were performed in a high-pressure and high-temperature reactor system, which was previously described (5). The flow of gas feeds (H₂ or N₂) was controlled through a gas flow meter, and liquid feeds (metal porphyrin solutions) was pumped into the reactor and mixed with hydrogen at the top of the reactor tube. The reactor tube had a length of 50cm and inside diameter of 0.6cm, and it was packed with 20-40 mesh inert silica. Although the temperature distribution of the reactor tube was not uniform, there was a constant temperature zone of about 5 mL in the middle of the reactor tube. Therefore this zone was used as the working section. The system operated in a down flow mode.

HDM experimental conditions in the absence of a catalyst are listed in table 1, and the volume ratio of H₂ to liquid feed is 250:1 for all the runs. In addition, in order to examine whether there are thermolysis reactions for NiOEP and VOOEP at the temperature ranging from 613K to 653K, H₂ is replaced with N₂. The volume ratio of N₂ to liquid feed is also 250:1, and the other experimental conditions are given in table 2.

Liquid samples were subjected to atomic absorption spectrophotometry (AAS) and ultraviolet-visible (Uv-vis) spectrophotometry. A flame atomic absorption spectrophotometer (WFX-1F2B) was used to determine the total nickel concentration and a nonflame atomic absorption spectrophotometer (HITACHI Z-8000) with a graphite furnace system the total vanadium content. The metal porphyrin or porphyrinic metal concentration measurement was made on an Uv-vis spectrophotometer (VARIAN CARY 50) according to the characteristic peaks of metal porphyrins, and

simultaneously their electronic spectra were recorded on this instrument.

Table 1 HDM Conditions

Run no.	Porphyrin type	Ni or V concn in feeds, ppm	Temp, K	H ₂ pressure, MPa
1	NiOEP	7.06	613	9
2	NiOEP	7.92	633	9
3	NiOEP	8.46	653	9
4	NiOEP	7.92	633	6
5	NiOEP	7.92	633	3
6	VOOEP	8.21	633	9

Table 2 Thermal Reaction Conditions

Run no.	Porphyrin type	Ni or V concn in feeds, ppm	Temp, K	N ₂ pressure, MPa
7	NiOEP	2.40	633	6
8	NiOEP	2.40	653	6
9	VOOEP	2.44	633	6

Results and Discussion

In our experiments, there was no gas resultant and the liquid product yield was 100w%. Metal porphyrin conversion (MPC) was defined as

$$MPC = \frac{C_{MP,feed} - C_{MP,product}}{C_{MP,feed}} \times 100\%$$

where C_{MP,feed} represents the metal porphyrin concentration in feeds and C_{MP,product} the metal porphyrin concentration in liquid products. The demetallation yield (DMY) of metal porphyrin was defined as

$$DMY = \frac{C_{M,feed} - C_{M,product}}{C_{M,feed}} \times 100\%$$

where C_{M,feed} represents the metal concentration in feeds and C_{MP,product} the metal concentration in liquid products.

**Table 3 MPC and DMY
(The liquid feed flow was 0.3mL/min)**

Run no.	MPC	DMY
1	29.1	27.5
2	33.4	30.6
3	47.0	39.5
4	27.7	25.8
5	19.9	18.3
6	38.5	34.6
7	0	0
8	0	0
9	0	0

For all the runs, when the liquid feed flow was 0.3ml/min, MPC and DMY are given in table 3. In the presence of H₂, even without a catalyst, the two metal porphyrins can be demetallated. By contrast, when H₂ was replaced with N₂, their MPC and DMC are both zero, and they don't decompose thermally. Based on the above findings, it is conclude that H₂ plays a key role during the demetallation reaction of the two metal porphyrins in the absence of a catalyst.

For NiOEP and VOOEP, although MPC and DMY of the non-catalytic HDM are lower than that of the catalytic HDM (5-6), their demetallation reaction mechanism appears to be same, i.e., the sequential HDM mechanism. This would be confirmed by the following facts.

For every HDM run, MPC is always higher than DMY (table 3). This means that the concentration of total metal is larger than that of porphyrinic metal in liquid products, but the former is identical with the latter in feeds. Obviously there are newly formed metallorganics in liquid products. Figure 1 and 2 are the typical Uv-vis spectra of the feed and the liquid product during the non-catalytic HDM of NiOEP

respectively. Evidently, a new peak at 615nm occurs for the product (figure 3). Similarly, the typical Uv-vis spectra of the feed and the liquid product are shown respectively in figure 3 and 4 during the non-catalytic HDM of VOOEP, and a new peak at 629nm appears for the product (figure 4). It is believed that the peak at 615 nm is of nickel octaethylchlorin and the peak at 629 nm is of vanadyl octaethylchlorin. The nickel or vanadyl octaethylchlorin is a dihydroporphyrin in which the peripheral double bond of one pyrrole group is hydrogenated; their structures are shown in figure 5.

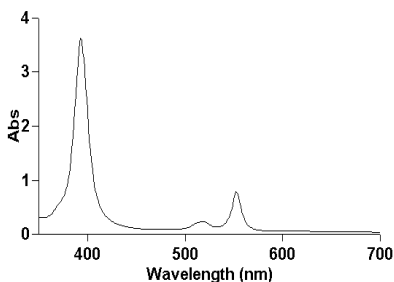


Figure 1. Uv-vis Spectrum of the NiOEP Feed (Diluted with Liquid Paraffin)

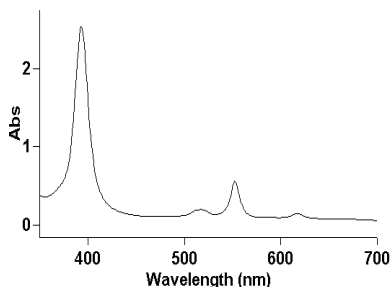


Figure 2. Uv-vis Spectrum of the Liquid Product during the Non-catalytic of NiOEP (Diluted with Liquid Paraffin)

To provide much proof that the two new peaks belong to nickel and vanadyl chlorins respectively and they are the main stable intermediates during the non-catalytic HDM, we separated the reaction intermediates from liquid products by alumina adsorption chromatograph. The detailed procedure is as follows: (a) 25mL product was diluted with 25 mL n-heptane, then placed on the top of neutral alumina (100~200mesh, 1% H_2O) in a glass column (15X250 mm). As the purple liquid completely entered the alumina column, a little fresh alumina was placed on its top to cover it. (b) At first, elution with n-heptane removed a colorless metal-free fraction in which the unreacted liquid paraffin may be concentrated, and a purple fraction containing metal was adsorbed on the upper portion of the column. Secondly, when toluene (for the product of NiOEP HDM) or 1:1 dichloromethane/toluene (for the product of VOOEP HDM) was used to elute the purple fraction, it was made into two colored fractions. A blue fraction for NiOEP or a green fraction for VOOEP came out of the column firstly, and a red band then was effluent.

The above colored fractions were subjected to Uv-vis and MS analysis. The spectra of the red fractions are the same as that of feeds. The spectrum of the blue fraction is shown in figure 6, and the spectrum of the green fraction is given in figure 7. In figure 6, the ratio of the Soret band (397nm) to the 615nm band is about 2, which was found to be one of the most typical characteristics of nickel octaethylchlorin (7). MS measurement indicated that NiOEP and the blue fraction have the molecular weights of 590 and 592 respectively,

and VOOEP and the green fraction have the molecular weights of 600 and 602 respectively.

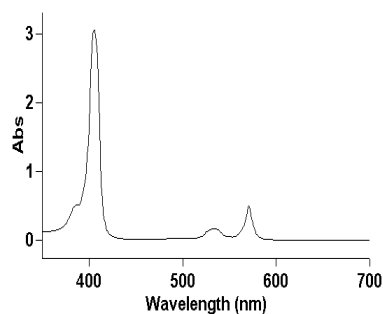


Figure 3. Uv-vis Spectrum of the VOOEP Feed (Diluted with Liquid Paraffin)

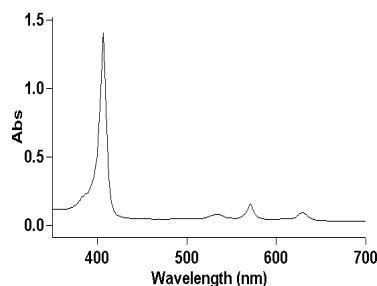


Figure 4. Uv-vis Spectrum of the Liquid Product during the Non-catalytic of VOOEP (Diluted with Liquid Paraffin)

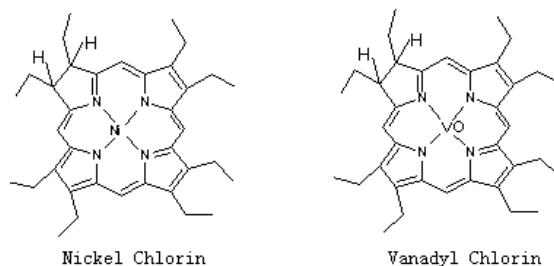


Figure 5 Structures of Nickel and Vanadyl Octaethylchlorin

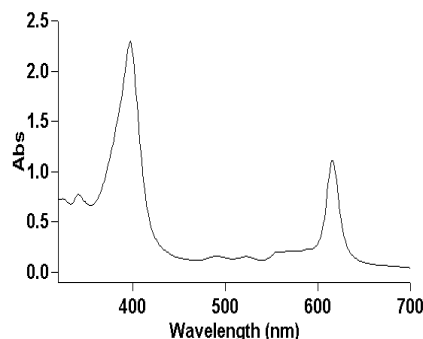


Figure 6. Uv-vis Spectrum of Nickel Octaethylporphyrin in Toluene

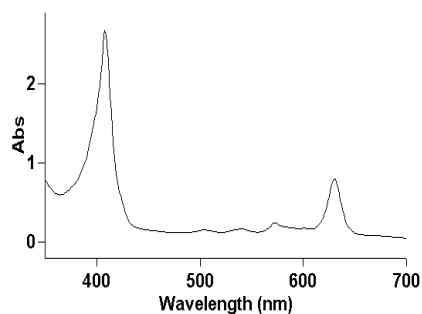


Figure 7. Uv-vis Spectrum of Vanadyl Octaethylporphyrin in dichloromethane/toluene

Table 4. C_M , $C_{M,MP}$ and $C_{M,MC}$ of the Liquid Products of Run 3

Liquid feed flow, mL/min	C_M , ppm	$C_{M,MP}$, ppm	$C_{M,MC}$, ppm
0.1	2.94	2.47	0.46
0.3	5.14	4.49	0.62
0.6	6.30	5.73	0.58
1.0	7.13	6.68	0.48
2.0	7.76	7.42	0.38

The separated metal chlorins were dissolved in the liquid paraffin. Their absorption coefficients were determined through AAS and Uv-vis. According to the coefficients, the chlorinic metal concentration was measured during the non-catalytic HDM. The sum of porphyrinic metal concentration ($C_{M,MP}$) and chlorinic metal concentration ($C_{M,MC}$) is approximately equal to the total metal content (C_M) in liquid products, which is shown in table 4. All the above findings confirm that the metal chlorins are the main stable intermediates during the non-catalytic HDM of NiOEP and VOOEP.

Conclusions

In the presence of N_2 , NiOEP and VOOEP are stable at the temperature ranging from 513K to 653K. In H_2 , however, even without a catalyst, they are not stable and metals are demetallated. The non-catalytic HDM reaction mechanisms of NiOEP and VOOEP are similar to their catalytic HDM mechanisms, firstly being the hydrogenation of metal porphyrin to metal chlorin, followed by the hydrogenolysis of metal chlorin which fragments ring system and results in demetallation.

Acknowledgement. The authors thank B. H. Zhang, L. Q. Wang for their effective assistance in experimental work, and are grateful to SINOPEC for necessary fund support.

References

- (1) Hung, C. W.; Wei, J. *Ind. Eng. Chem. Process Des. Dev.* **1980**, 19 (2), 250.
- (2) Agrawal, C. W.; Wei, J. *Ind. Eng. Chem. Process Des. Dev.* **1984**, 23 (3), 505.
- (3) Ware, R. A.; Wei, J. *J. of Catal.* **1985**, 93(1), 100.
- (4) Bonne, R. L. C.; van Steenderen, P. V.; van Langeveld, A. D.; Moulijin, J. A. *Ind. Eng. Chem. Res.* **1995**, 34, 3801.
- (5) Xu, H.; Que, G. H.; Yu, D. Y.; Wang, Z. X. Prepr. Pap. – *Am. Chem. Soc., Div. Pet. Chem.* **2001**, 46(4), 84.
- (6) Xu, H.; Yu, D. Y.; Wang, Z. X.; Que, G. H. *Acta Petrolei Sinica (Petroleum Processing Section)* **2001**, 17(4), 18
- (7) Fuhrhop, J. H. Z. *Naturforsch* **1970**, 25b, 255

MORPHOLOGY AND REACTIVITY OF BED MATERIALS IN PFBC BOILER AT DIFFERENT LOAD

F. Ishom¹⁾, T. Harada²⁾, T. Aoyagi³⁾, Y. Korai¹⁾, I. Mochida¹⁾

¹Institute of Advanced material Study, Kyushu University

²Nishinippon Environmental Energy

³Kyushu Electric Power

Abstract:

Bed materials in pressurized fluidized bed combustion (PFBC) at various combustion conditions were characterized by SEM and TGA to describe their morphology and reactivity. 270 MW output conditions were found to keep bed material uniform, whereas 285 MW output conditions produced sintered egg (SE), sintered grain (SG), and unburnt char (UC) among the bed materials. Normal fluidization of uniform bed materials mainly at 270 MW output level combustion. Poor fluidization at 285 MW caused several types of adhering and agglomerating of bed materials was produced in the boiler. Local heating during poor fluidization was suggested to cause the formation spherical particle through the melting and melted surface particle of SE to be flat. Fine particles of aluminasilicate adhered to the melted surface to form porous surface.

Introduction

Pressurized fluidized bed combustion (PFBC) of coal has been recognized as an advanced coal firing process to achieve high thermal efficiency through combined cycles, high combustion efficiency for poor coals of low reactivity, and environmental protection using calcium minerals as bed material [1].

Several PFBC plants have been operated in Japan. There are reported several problems in PFBC operation. One of the problems is reported poor fluidization at the high-level load operation producing agglomerates among bed materials.

In the present report, bed materials at two combustion conditions (270 and 285 MW outputs) were recovered from the bottom of a commercial PFBC boiler to be characterized by SEM-EDAX and TGA in terms of its morphology and weight loss change by the heat treatment. Through such analysis, mechanism of formation is discussed to propose way how to reduce such problems.

Experimental

Bed materials (BM) in PFBC operated at load levels 270 and 285 MW were recovered from the bottom of 360 MW PFBC boiler were used as samples. Uniform particle of BM at 270 MW output level was called BM270. Bed materials at 285 MW output level were separated by hand picking up into similar particles being called BM285. BM285 carried sintered egg (SE), sintered grain (SG), and unburnt char (UC). BM270, BM285, SG, SE, and UC were characterized by SEM-EDAX (JEOL JSM-6320F) and TGA (Seiko Instruments 220).

Result and Discussion

270 MW output level

Bed materials produced from PFBC at 270 MW output level contained uniform particles as shown in Figure 1a. Morphology of BM270 shows porous on the surface of the CaCO₃ as shown in Figures 2a and 2e. Around 1 μm calcium aluminasilicate particles were melted and bonded together to form outer face of BM270 particle. Uniform surface of BM270 showed no local heating during combustion. TG/DTG profile of BM270 showed weight loss 35%wt at 700°C suggesting CaCO₃ decomposition. BM270 commonly contained CaCO₃ and small amount of calcium aluminasilicate on the

outer surface. Limestone as raw bed materials of PFBC was suggested to be core particle of BM270. Its surface react with SO_x released from coal combustion and was covered by aluminasilicate particle from coal ash.

285 MW output level

285 output level of PFBC produced several kinds of bed materials which could be separated by hand picking up BM285, carried sintered egg (SE), sintered grain (SG), and unburnt char (UC) as shown in Figure 1b

Major part of BM285 carried similar outer face to that of BM270, carrying porous faces. TG/DTG showed 40% weight loss at 700°C like BM270, indicating major core of limestone. Some spheres were unusually observation on surface of BM285. Such spheres were of CaO, SiO₂ and Al₂O₃ fine particles, which were fused together to form sphere and to be adhered onto the surface of limestone.

Sintered egg (SE) found at BM285 was shown in figure 1c. The morphology of SE shows melted surface with several fine particles adhered on the outer surface. TG/DTG profile of SE shows only 5% weight loss during heating in the air atmosphere. Small amount of CaCO₃ contained in SE. Melted surface of calcium aluminasilicate suggested fusion and adhesion of fine particle of CaO, SiO₂ and Al₂O₃ to for SE at the high indicating temperature due to local heating.

Figure 1d shows sintered grain (SG) particle. Very fine particle (around 0.1 μm) sintered and bonded together to form SG. No weight loss occurred during heat treatment to 1000°C in air atmosphere. A very fine particle of aluminasilicate was suggesting to form SG.

Unburnt char (UC) was also picked up among BM285. It was combusted completely in TGA. Insufficient oxygen or short time residence in the boiler may cause the production of UC.

References

- [1] Anderson, J., Anderson, L., Energy and Fuel, 1998; 39(3): p.207
- [2] Abe R, Sasatsu H, Harada T, Misawa N, Saito I, Fuel, 2001; 80(1): p.135-144.
- [3] Qiu, Kuanrong; Steenari, Britt-Marie, Energy and Fuel, 2000; 14(5): p.973-979

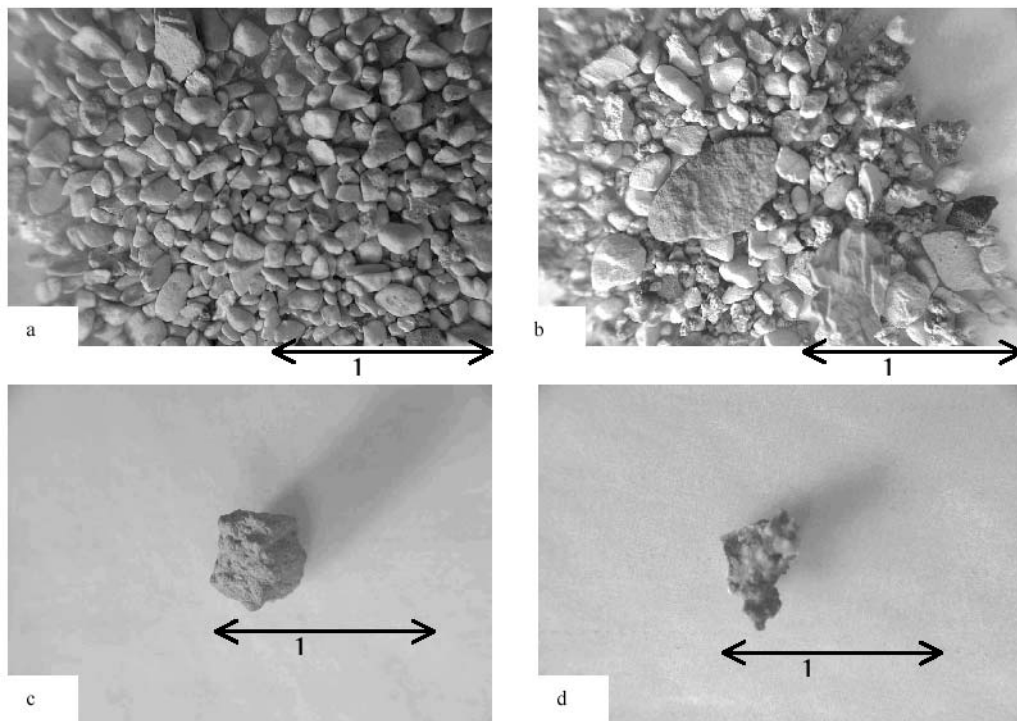


Figure 1. Photograph of bed material (BM) recovered from PFBC boiler: (a) BM 270/360 MW, (b) BM 285/360 MW, (c) Sintered egg, and (d) Sintered grain.

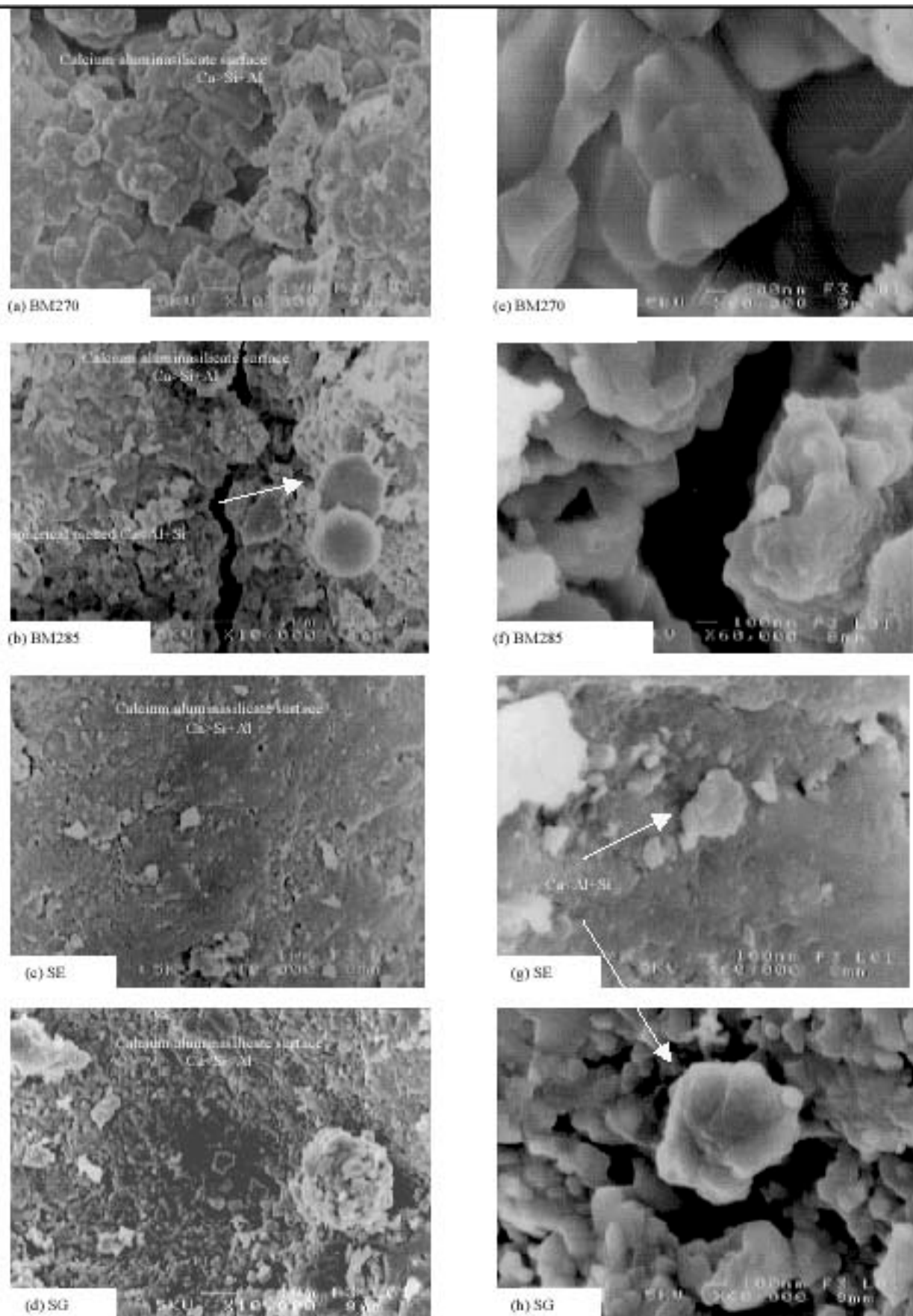


Figure 2. SEM photograph of: 10,000 x magnification of (a) BM270, (b) BM285, (c) SE, and (d) SG; and 60,000 x magnification of (e) BM270, (f) BM285, (g) SE, and (h) SG

Thermal-cracking and catalytic hydro-cracking reaction of tetralin and normal eicosane with steady isotope

SHI Bin QUE GuoHe

(National Laboratory of Heavy Oil Processing, University of Petroleum, Dongying, 257062;PRC)

Introduction

Hydrogen donors were used in coal liquefaction(1) and residue conversion(2), in which hydrogen donors were important in inhibiting the coke formation. Because coal and petroleum residue structures have been unclear, a study of the reactions of coal- or petroleum residue-related model compounds is a powerful approach in hydrogen-transfer between hydrogen donors and complex macromolecule. This paper reports the effects of hydrogen donor and H₂ on thermal-, hydro-, catalytic hydrocracking of n-C₂₀ and hydrogen transferring between normal hydrocarbon and hydrogen donor.

Experimental

Normal C₂₀ was used as reagent, and 1-methylnaphthelene (98%pure) as aromatic solvent, tetralinC₁₀H₁₂ (99.3%) as hydrogen donor, detuerated tetralin C₁₀D₁₂ (98%D, Aldrich provided) as deuterated H-donor for tracking the hydrogen-transfer between hydrogen donors and normal hydrocarbon. The experimental procedure was as literature (4). The reaction products were recovered with chloroform and analysed by GC and GC-MS.

Results and Discussion

Thermal-, hydro-cracking, catalytic hydro-cracking of n-C₂₀ was performed, while thermal- or hydro- cracking of n-C₂₀ in hydrogen donor (tetralin,THN) or aromatic solvent(1-methylnaphthelene ,1-MN) were also carried out as comparison . Distribution of the reaction products was displayed in Figure1. It seems that distribution in carbonic number of the products in the four cracking reaction have not changed, however, the catalytic hydrocracking of n-C₂₀ could crack more than hydrocracking and thermal cracking of n-C₂₀. On the

other hand, it is clear that in the presence of H-donor or aromatic solvent, especially in the presence of H-donor, inhibited cracking of n-C₂₀. What is different was that the ratio of n-alkanes to α-olefins in thermal cracking and thermal-cracking with aromatic solvent was about 1:1, and that in thermal-cracking in H-donor decreased to about 1:0.5. The proportion of α-olefins in hydrocracking of n-C₂₀ remained about 15~10% and hydrocracking of n-C₂₀ with H-donor hardly gave α-olefins. Catalytic hydrocracking of n-C₂₀ without or with THN brought about no α-olefins. It is obvious that hydrogen-in-gas and hydrogen provided from H-donor could have hydrogenated the olefins resulted from cracking of n-C₂₀ and the former could enhance cracking of n-C₂₀ and the latter could inhibit cracking.

Deuteron as steady isotope of hydrogen could be used to investigate the mechanism of hydrogen-transferring (3). In the following experiment, C₁₀D₁₂ was used as deuterated H-donor for tracking hydrogen-transferring between hydrogen donors and hydrocarbon. From Table2, it is found that deuterated H-donor existed a substantial isotopic kinetic effect in the thermal cracking system and that the isotopic kinetic effect was reduced in the hydrocracking and catalytic hydrocracking system. H- or D-donating yields at high temperature were more than in low temperature since more radicals could yield by high temperature and get scavenged by H-donor.

During initialization or propagation of the thermal radicals of n-C₂₀, hydrogen donation from tetralin for s scavenging thermal radicals of n-C₂₀ could strongly affect the thermal cracking of n-C₂₀. That is to say, the hydrogen from tetralin could scavenge the radicals of n-C₂₀ and the cracking of n-C₂₀ would be inhibited. This reaction could also affect hydrocracking and catalytic hydrocracking of n-C₂₀.

Fig 2~4 show the GC-MS of the recovered n-C₂₀. From the M+1or M+2 peak, there existed one deuterium in the paraffinic chain, except that there were two deuteriums in the catalytic hydrocracking system. It is clear that deuterium was from deuterium-donor and could be used to scavenge radicals of n-C₂₀. The MS of the recovered

C₁₀D₁₂ showed C₁₀D₁₂ had experienced H-D exchange in Fig 5~7. Except the molecular peak 144, the peaks from 143 to 132 were the molecular peaks of tetralin, which had experienced H-D exchange. It is clear that H-D exchange in catalytic hydrocracking system was the most, and in hydrogen atmosphere was stronger than in nitrogen atmosphere.

²H-NMR analysis of D₁₂-THN, which was separated and recovered by small-scale liquid chromatography showed that the 2.63ppm peak of D α of recovered D₁₂-THN, was smaller than that of 1.70ppm D β from Fig 8. The ratio of D α and D β was 0.856 (thermal cracking), 0.726 (hydro-cracking), 0.695 (catalytic hydro-cracking). It is clear that the dehydrogenation of tetralin was selective and the α -hydrogen of naphthenic ring was easier to dehydrogenate than the β -hydrogen.

¹H-NMR analysis of D₁₂-THN displayed the same trend of the dehydrogenation of tetralin. It is shown that dehydrogenation of tetralin was stepwise and α hydrogen could be abstracted by the radicals and then β could be continued, when H₂ atmosphere could rehydrogenation on the abstracted tetralin, this is the "hydrogen shuttle" in the catalytic hydrocracking system.

The scheme of reaction mechanism between eicosane and D₁₂-THN in the cracking system would be suggested in Fig.9. Fig.9 shows the H-D exchange reaction between tetralin and n-C₂₀ in the thermal cracking have been transformed into the rehydrogenation of tetralin in hydrocracking and catalytic hydrocracking system under H₂ atmosphere.

Conclusion

1. It is found that the effect of hydrogen donor was inhibition of cracking reaction and hydrogen atmosphere and dispersed catalysts were enhancement of cracking.

2. Hydrogen donor or H₂/dispersed catalyst could perform the saturation of the radicals and decrease the yield of olefins.

3. Inhibition of cracking of normal hydrocarbon with tetralin was

ascribed to the dehydrogenation of tetralin for scavenging the thermal radicals.

4. There existed a substantial isotopic kinetic effect of deuterated tetralin in the cracking system under nitrogen and under hydrogen, and the isotopic kinetic effect could reduce in the cracking system under hydrogen.

5. Hydrogen (or deuterium) donation of hydrogen donor depended on reaction temperature and number of radicals in reaction system.

6. The dehydrogenation of tetralin was stepwise and the α -hydrogen of naphthenic ring was easier to dehydrogenate than the β -hydrogen.

Acknowledgement. The authors thank Wang LuoQiu and Wang Jing for their effective assistance in experimental work, and are grateful to University of Petroleum and National Laboratory of Heavy Oil Processing for fund support.

References:

- (1). Yanlong Shi, Lian Shao, Willian F. Olson Coprocessing coal with hydrogenated vacuum pyrolyzed tire oil [J]. Fuel processing Technology, 1999,(58):135~150
- (2). Shi Bin, Li PeiPei, Que GuoHe. New developments in deep hydro conversion of heavy oil residues with dispersed catalysts [J] Preprints, div. fuel chem., ACS, 1998, 43(3): 558-562.
- (3). R. P. Skowronski, and J. J. Ratto, I. B. Goldberg et al Hydrogen incorporation during coal liquefaction [J] Fuel 1984(63) 4,440-448.
- (4). Shi Bin, Wang Luoqiu, Weng Ping, et al. Reaction of H-donor and paraffinic series as model compounds for residue oil with steady isotope method [J] J. of Fuel Chem. and Tech. (China) 2001(29) 5,400-403.

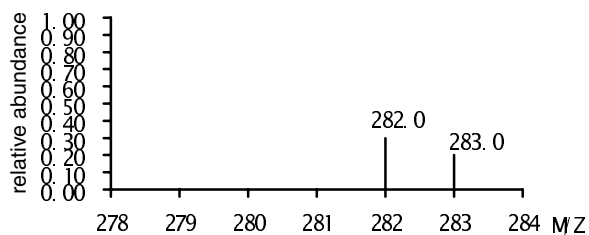


Figure2 M+1 peak of recovered eicosane scavenged by deuterium under nitrogen

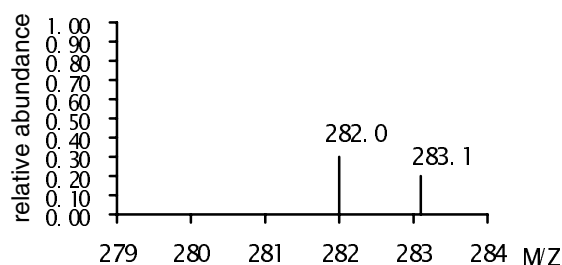


Figure3 M+1 peak of recovered eicosane scavenged by deuterium under hydrogen

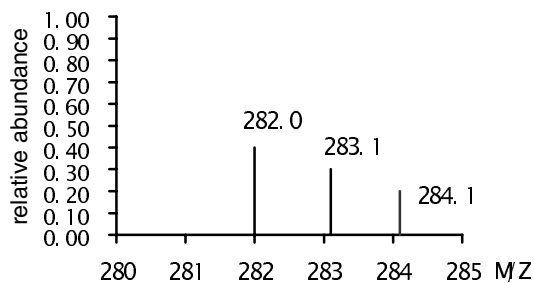


Figure 4 M+1 and M+2 peak of recovered eicosane scavenged by deuterium in catalytic hydrocracking system

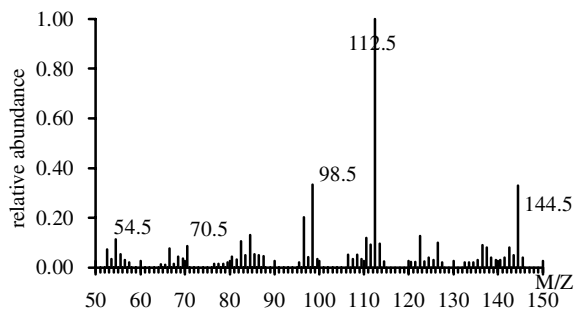


Figure5 MS of recovered D₁₂-THN in thermal-cracking system

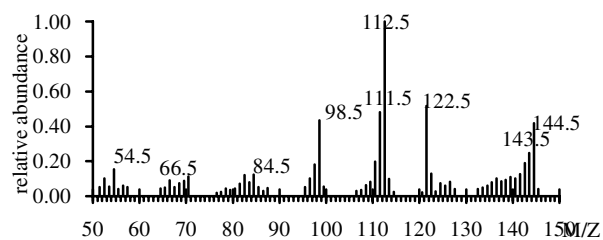


Figure 6 MS of recovered D₁₂-THN in hydrocracking system

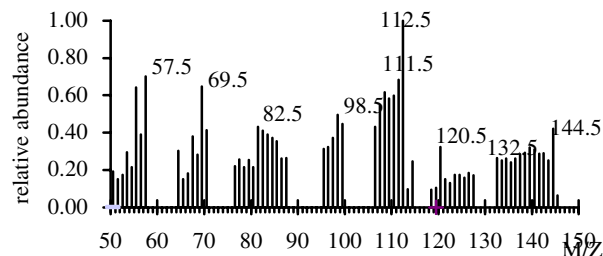


Figure 7 MS of recovered D₁₂-THN in catalytic hydrocracking system

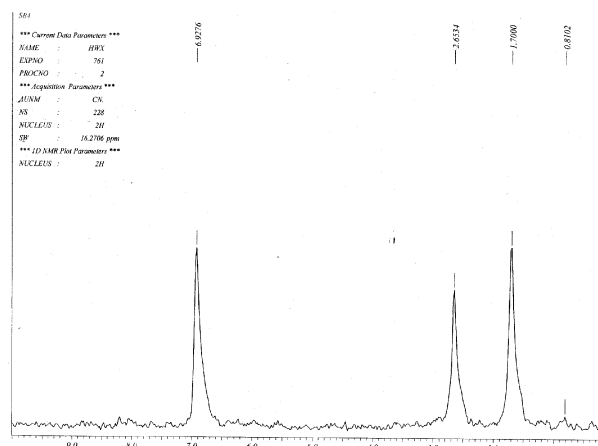


Figure8 ²H-NMR of recovered D₁₂-THN in the cracking system

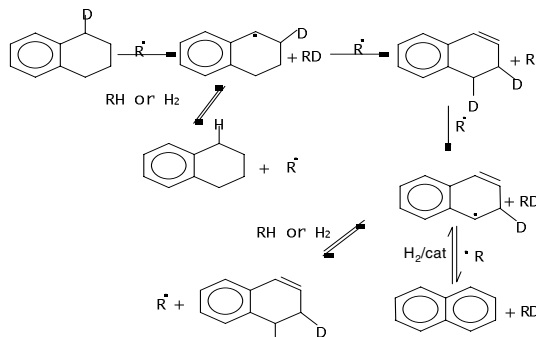


Figure9 Scheme of reaction mechanism between eicosane and D₁₂-THN in the cracking system

Table 1 Hydrogen(or deuterium) donating yields of THN reacted with eicosane /W%

T(°C)	N ₂		H ₂		H ₂ +Mo	
	H ₁₂ -THN	D ₁₂ -THN	H ₁₂ -THN	D ₁₂ -THN	H ₁₂ -THN	D ₁₂ -THN
430	6.14	2.96	18.43	10.31	11.79	8.38
440	11.62	7.17	30.36	22.78	23.10	19.45

Note: eicosane /THN=0.100 g /0.100g; initial nitrogen pressure 7.0Mpa; durance time:1hr; Mo/ eicosane=1.0w%

Table2 ²H-NMR of recovered D₁₂-THN experienced different hydrocracking

	D ₁₂ -THN D α	D ₁₂ -THN D β	D ₁₂ -THN A _D
Peak shift (ppm)	2.63	1.70	6.93
thermal-cracking system	0.267	0.312	0.421
hydro-cracking system	0.244	0.336	0.420
catalytic hydro-cracking system	0.248	0.357	0.395

Table 3 ¹H-NMR of recovered D₁₂-THN experienced different cracking

	D ₁₂ -THN H α	D ₁₂ -THN H β	D ₁₂ -THN A _H
Peak shift (ppm)	2.60	1.70	7.02
thermal-cracking system	0.40	0.35	0.25
hydro-cracking system	0.46	0.35	0.26
catalytic hydro-cracking system	0.40	0.30	0.35

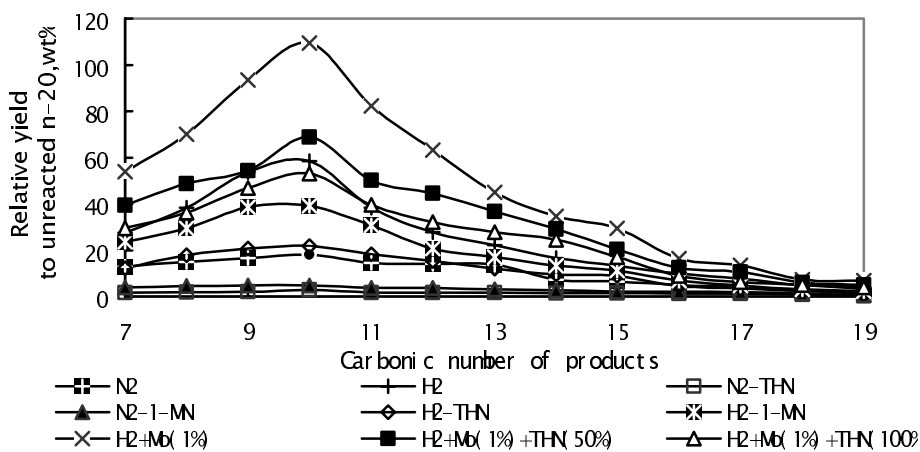


Figure1 Distribution of carbonic number in thermal-, hydro-and catalytic cracking of n-C₂₀ in 440 °C